DOI: 10.13009/EUCASS2017-476

Numerical investigation of transpiration cooling with uniformly and non-uniformly simulated injection

Wolfgang Dahmen⋆*, Valentina König*⋆†*, Siegfried Müller*⋆ *and Michael Rom*⋆
⋆*IGPM, RWTH Aachen University*
Templergraben 55, 52056 Aachen, Germany
{dahmen, koenig, mueller, rom}@igpm.rwth-aachen.de
†Corresponding author

Abstract

The present paper deals with a numerical investigation of transpiration cooling which is an innovative concept for reducing the high thermal loads of rocket thrust chambers. The hot gas in the channel flows over a porous ceramic matrix composite (CMC) material through which the coolant is injected. The focus is set on studying the difference between cooling gas injection simulated (i) uniformly by using an average coolant mass flux and (ii) non-uniformly by prescribing outflow velocity data measured experimentally along a porous medium in small intervals. The influence on a subsonic turbulent hot gas channel flow is investigated.

1. Introduction

Transpiration cooling is a promising concept for the reduction of thermal loads at walls in future space transportation systems. It is based on the injection of a coolant into a boundary layer through a porous material. The injection is driven by the pressure difference between the hot gas flow and the coolant reservoir. The hot gas in the boundary layer is displaced and a protective layer with lower temperature is formed on the surface of the cooled structure. An accompanying effect is the significant reduction of the resulting wall heat flux and the skin friction.[9]

Compared with other active cooling techniques such as film or effusion cooling, transpiration cooling might offer advantages regarding the formation of stable films, see Linn et al.[16,17] and Linn et al.,[15] and the cooling efficiency. With the availability of permeable ceramics, in particular composite carbon/carbon (C/C) materials, investigated for instance by Selzer et al.,[22] the development of transpiration-cooled CMC combustion chambers is a recent research topic, see for instance Ortelt et al.[20] or Herbertz et al.[10] Transpiration cooling with CMC materials was also investigated by Langener,[13] Langener et al.[14] and Schweikert et al.[21] at sub- and supersonic speeds. Numerical simulations of hot gas flows exposed to transpiration cooling were conducted by Jiang et al.[12] and more recently by Liu et al.[18] The objective of these simulations was the investigation of the effect of the cooling gas injection on the hot gas flow, especially on the boundary layer.

In recent work[4–7,9] transpiration cooling in a subsonic turbulent channel has been investigated numerically using a two-domain approach. The turbulent hot gas channel flow is modeled by the compressible Reynolds-averaged Navier-Stokes equations whereas the porous medium flow model is modeled by the continuity equation, the Darcy-Forchheimer equation and two temperature equations for both fluid and solid material. These models are coupled by interface conditions. Two separate solvers are used, namely, the adaptive parallel finite volume flow solver Quadflow[3] and a parallel finite element solver using the deal.II library[2] for the hot gas flow and for the porous medium flow, respectively. In the following, we will refer to the two solvers as the flow solver and the porous medium solver, respectively. The coupling of these solvers is realized in a weak sense, i.e., both solvers are applied alternatingly where in each iteration the respective solver is converged to a steady state with respect to the boundary conditions at the interface provided by the solution of the other solver. This process is continued until no further changes in both solutions occur.

So far, the focus has been on the development of appropriate coupling conditions.[6,7,9] For validation, simulation results were compared with experimental data for the porous medium flow from Langener et al.[14] and with hot gas temperature and velocity boundary layer profiles from Schweikert et al.[21] Two- and three-dimensional simulations have been performed. In particular, the influence of the cooling gas injection on the boundary layer in the hot gas has been investigated.[7] Besides air injection into air also argon has been used as a coolant.[5]

DOI: 10.13009/EUCASS2017-476

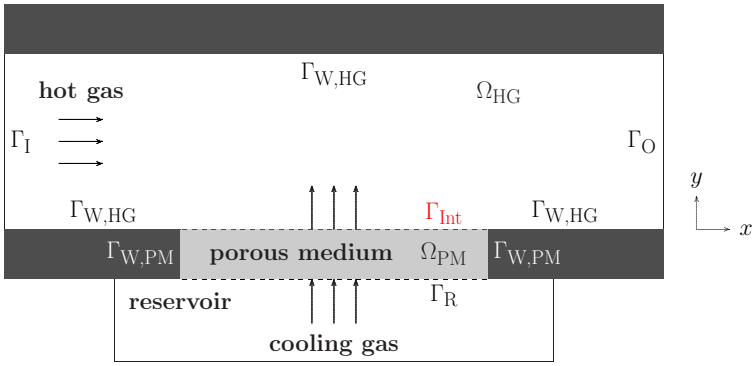

Figure 1: Configuration of coupled fluid-porous medium problem.

In the aforementioned investigations a spatially constant mass flux has been used to determine the local outflow velocities at the coupling interface. However, due to the porosity of the porous medium the mass flux will be locally varying in space. This has been recently investigated in experiments performed by Selzer et al.[23] where the mass flux has been measured at the surface of the porous material. In the present work, we perform 2D simulations where we prescribe local outflow velocities that are computed from the spatially varying mass flux determined in the experiment. The numerical investigations concentrate on the comparison of 2D simulation results obtained by simulating *uniform* and *non-uniform* injection which means using a *spatially constant* and a *spatially variable* mass flux, respectively. For the computations both the cooling gas and the hot gas in the channel are air.

The paper is structured as follows: The physical modeling of the turbulent hot gas channel flow and the porous medium flow as well as suitable boundary conditions and the coupling of the two solvers are discussed in Sect. 2. In Sect. 3, the numerical method for solving the coupled problem is described. Numerical results for a coupled two-dimensional simulation are presented in Sect. 4. A summary of the main results and an outlook on future work in Sect. 5 conclude the paper.

2. Physical Modeling

The configuration for the coupled problem of turbulent hot gas channel flow and porous medium flow is illustrated in Fig. 1. The models for the hot gas flow and for the porous medium flow are briefly discussed in Sects. 2.1 and 2.2, respectively. This includes the boundary conditions and the initialization for the particular flow domain. The coupling conditions, i.e., the boundary conditions on the interface Γ_{Int}, are described in Sect. 2.3. Detailed information on the governing equations for the hot gas flow and the porous medium flow can be found in.[6,7,9]

2.1 Hot Gas Flow

The hot gas flow is described by the compressible Reynolds-averaged Navier-Stokes equations, complemented by the Wilcox $k-\omega$ turbulence model.[24] This leads to a system of equations which is solved for the conservative flow quantities

$$\vec{U}_{HG} = \left(\bar{\rho}, \bar{\rho}\tilde{\vec{v}}, \bar{\rho}\tilde{E}, \bar{\rho}\tilde{k}, \bar{\rho}\tilde{\omega}\right) . \tag{1}$$

Here, $\bar{\rho}$ is the Reynolds-averaged density and $\tilde{\vec{v}}$, $\tilde{E}$, $\tilde{k}$ and $\tilde{\omega}$ are the Favre-averaged values for the velocity, the total energy, the turbulence kinetic energy and the turbulent dissipation, respectively.

2.1.1 Boundary Conditions

At the inflow boundary Γ_I, the velocity and the temperature of the subsonic turbulent channel flow are prescribed by

$$\vec{v} = \vec{v}_\infty, \quad T = T_\infty \qquad \text{on } \Gamma_I , \tag{2}$$

where the subscript ∞ indicates the inflow conditions. The static pressure on Γ_I is extrapolated from the interior flow domain.

At the outflow boundary Γ_O, only the pressure is prescribed by setting

$$p = p_\infty \qquad \text{on } \Gamma_O . \tag{3}$$

DOI: 10.13009/EUCASS2017-476

For the walls $\Gamma_{W,HG}$ of the channel, isothermal as well as adiabatic walls can be used. Upstream of the porous medium, an isothermal wall can account for cold walls (in relation to the adiabatic wall temperature) which can occur in experiments due to the thermal behavior of a test section.[21] Downstream of the cooling gas injection, the cooled wall is modeled as an adiabatic wall to account for the changing wall temperature due to the cooling.

2.1.2 Initialization

All initial hot gas flow quantities in the domain Ω_{HG} can be computed from the inflow conditions. For this purpose, the density ρ_∞, the temperature T_∞, the Mach number M_∞, the turbulence intensity $Tu_\infty = \sqrt{2/3\,\tilde{k}_\infty}/v_{x,\infty}$ (where $v_{x,\infty}$ is the velocity component in flow direction x) and the ratio of the turbulent dynamic viscosity to the laminar dynamic viscosity $(\mu_t/\mu)_\infty$ are prescribed.

2.2 Porous Medium Flow

The pressure-driven laminar flow through the porous medium is modeled by taking into account the continuity equation, the Darcy-Forchheimer momentum equation and two heat equations for the solid and the fluid part of the porous material, respectively. The splitting into two heat equations is necessary to model thermal non-equilibrium. The resulting system of equations is solved for the variables

$$\vec{U}_{PM} = \left(\rho_f, \vec{v}, T_s, T_f\right), \tag{4}$$

denoting the fluid density, the Darcy velocity, the solid temperature and the fluid temperature, respectively. The Darcy velocity $\vec{v}$ is the average velocity with respect to a volume element containing both solid and fluid material. It is defined by $\vec{v} = \varphi\vec{V}$, where φ is the porosity and $\vec{V}$ the intrinsic average velocity obtained by averaging over a volume element consisting only of fluid.

2.2.1 Boundary Conditions

The first boundary condition for the inflow boundary Γ_R, where the coolant enters the porous medium from the reservoir, concerns the fluid density ρ_f. Its value is computed by the equation of state for a thermally and calorically perfect gas which in general form reads $p = \rho R\,T$ with the specific gas constant R, here yielding

$$\rho_f = \frac{p_c}{R\,T_{f,R}} =: \rho_{f,R} \qquad \text{on } \Gamma_R, \tag{5}$$

where p_c is the constant reservoir pressure. The temperatures on Γ_R are determined by

$$T_s = T_b, \quad T_f = T_{f,R} \qquad \text{on } \Gamma_R, \tag{6}$$

where T_b is the temperature of the solid on the backside of the porous material and the fluid reservoir temperature $T_{f,R}$ is determined by the heat flux balance

$$(1-\varphi)\,(\boldsymbol{\kappa_s}\nabla T_s)\cdot\vec{n} = c_{p,f}\,\rho_{f,R}\,v_y\left(T_{f,R} - T_c\right) \qquad \text{on } \Gamma_R, \tag{7}$$

cf.[19] In the initial stage we set $\nabla T_s = \mathbf{0}$ and $T_{f,R} = T_c$, later on ∇T_s is computed from the simulation. Here, $\boldsymbol{\kappa_s}$ is the heat conduction tensor and $c_{p,f}$ is the specific heat capacity of the fluid. The component v_y of the Darcy velocity $\vec{v}$ is the component in flow direction of the cooling gas, i.e., normal to the inflow boundary. The normal vector $\vec{n}$ points into the porous medium domain. The coolant temperature T_c is measured at one position in the reservoir (and not at the backside of the porous material) and is therefore a constant in the simulation.

The side walls denoted by $\Gamma_{W,PM}$ are set to be adiabatic, i.e.,

$$\nabla T_s\cdot\vec{n} = 0, \quad \nabla T_f\cdot\vec{n} = 0 \qquad \text{on } \Gamma_{W,PM}. \tag{8}$$

From a physical perspective, the normal component of $\vec{v}$ must vanish on $\Gamma_{W,PM}$, i.e.,

$$\vec{v}\cdot\vec{n} = 0 \qquad \text{on } \Gamma_{W,PM}, \tag{9}$$

whereas nontrivial tangential components have to be permitted since no viscous effects are taken into account in the Darcy-Forchheimer momentum equation.

DOI: 10.13009/EUCASS2017-476

2.2.2 Initialization

For an initial guess in the porous medium domain Ω_{PM}, suitable values have to be chosen. The density $\rho_{f,0}$ is determined by linearly interpolating the reservoir density and the hot gas density between Γ_R and Γ_{Int}, leading to

$$\rho_{f,0}(y) = \frac{p_c}{R\,T_c} + \frac{y - y_R}{y_{Int} - y_R}\left(\frac{p_{HG,Int}}{R\,T_{HG,Int}} - \frac{p_c}{R\,T_c}\right) \qquad \text{in } \Omega_{PM}\,. \tag{10}$$

In the case of uniform injection with a spatially constant mass flux, the normal component $v_{y,0}$ of the Darcy velocity is computed from the averaged coolant mass flux $\dot{m}_{c,\mathrm{avg}}$ measured in the experiment and the initial density distribution. For non-uniform injection, $v_{y,0}$ is set to the measured interface value and extended from the interface Γ_{Int} to the whole domain Ω_{PM} in normal direction. Overall, this can be written as

$$v_{x,0} = 0\,, \quad v_{y,0} = \frac{\dot{m}_{c,\mathrm{avg}}}{\rho_{f,0} A_c} \qquad \text{in } \Omega_{PM} \qquad \text{or} \tag{11a}$$

$$v_{x,0} = 0\,, \quad v_{y,0} = v_{y,\mathrm{measured}} \qquad \text{in } \Omega_{PM}\,, \tag{11b}$$

where A_c denotes the surface area of the porous material. The backside temperature T_b and the coolant reservoir temperature T_c are used as initial guess for the temperatures such that

$$T_{s,0} = T_b\,, \quad T_{f,0} = T_c \qquad \text{in } \Omega_{PM}\,. \tag{12}$$

2.3 Coupling Conditions on Γ_{Int}

By alternatingly applying the flow solver and the porous medium solver, solutions of one solver can be applied to compute boundary conditions for the other solver. Hence, both solvers are coupled and the resulting boundary conditions can be regarded as coupling conditions.

The velocity $\vec{v}_{PM}$ and the fluid temperature $T_{f,PM}$ obtained from the respective porous medium flow solution are used to compute the density ρ, the velocity $\vec{v}$, the total energy E and the turbulent dissipation ω in the hot gas flow at the interface Γ_{Int}:

$$\rho = \frac{p}{R\,T_{f,PM}}\,, \tag{13}$$

$$\vec{v} = \vec{v}_{PM}\,, \tag{14}$$

$$E = \frac{R}{\gamma - 1} T_{f,PM} + \frac{1}{2}\left|\vec{v}_{PM}\right|^2\,, \tag{15}$$

$$\omega = \frac{\rho\, u_\tau^2}{\mu} \frac{25}{\frac{v_{y,PM}}{u_\tau}\left(1 + 5\,\frac{v_{y,PM}}{u_\tau}\right)}\,. \tag{16}$$

The isentropic exponent γ in (15) is set to 1.4 for air. Coupling condition (16) originates from a modification of the Wilcox turbulence model to account for mass injection into the hot gas flow.[24] In this equation, $v_{y,PM}$ from the porous medium flow is the normal component of the injection velocity and $u_\tau = [\tau_w/\rho]^{1/2}$ is the friction velocity with the wall shear stress τ_w.

The pressure p_{HG}, the temperature T_{HG} and the temperature gradient ∇T_{HG} obtained from the respective hot gas flow solution are used to compute the normal component v_y of the Darcy velocity in the case of uniform injection and a heat flux balance incorporating the solid temperature gradient ∇T_s in the porous medium flow at the interface Γ_{Int}:

$$v_y = \frac{\dot{m}_{c,\mathrm{avg}}}{\rho_{Int}\, A_c} =: v_{y,Int} \quad \text{with} \quad \rho_{Int} := \frac{p_{HG}}{R\,T_f} \qquad \text{or} \tag{17a}$$

$$v_y = v_{y,\mathrm{measured}}\,, \tag{17b}$$

$$(1 - \varphi)\,(\boldsymbol{\kappa_s} \nabla T_s) \cdot \vec{n} = c_{p,f}\,\rho_f\, v_{y,Int}\,(T_f - T_{HG}) + \kappa_{HG} \nabla T_{HG} \cdot \vec{n}\,. \tag{18}$$

Note that in case of non-uniform injection no data from the hot gas flow are used such that (17b) is not a coupling condition anymore.

DOI: 10.13009/EUCASS2017-476

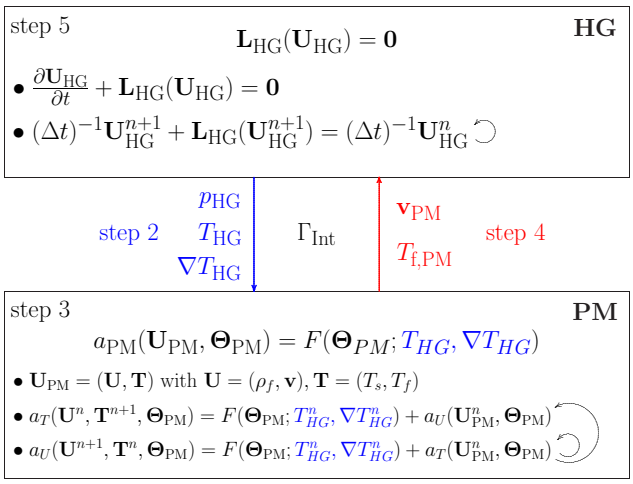

Figure 2: Illustration of the steps 2 to 5 of the iterative process for coupling hot gas and porous medium flow.

3. Numerical Method for Solving the Coupled Problem

For the solution of the coupled problem, we alternatingly and approximately solve the compressible Reynolds-averaged Navier-Stokes equations for the hot gas flow and the system for modeling the porous medium flow. This leads to solutions $\vec{U}_{HG}$ and $\vec{U}_{PM}$ in the two flow regimes. The developed iterative process is continued until

$$\left\| q_1(\vec{U}_{HG}^{n+1})\,|_{\Gamma_{Int}} - q_1(\vec{U}_{HG}^{n})\,|_{\Gamma_{Int}} \right\|_\infty \leq \varepsilon_1, \quad \left\| q_2(\vec{U}_{PM}^{n+1})\,|_{\Gamma_{Int}} - q_2(\vec{U}_{PM}^{n})\,|_{\Gamma_{Int}} \right\|_\infty \leq \varepsilon_2 \tag{19}$$

for flow quantities $q_1 \in \{\rho, T\}$ and $q_2 \in \{v_y, T_f\}$ and given tolerances $\varepsilon_1 > 0$ and $\varepsilon_2 > 0$. By applying these conditions, we monitor the variation of the flow quantities at the interface Γ_{Int} from one iteration to the next. If the maximal absolute difference between two iterations is small enough, the iterative process is stopped and the stationary *equilibrium solution* of the coupled system is obtained. The iterative process can be summarized as follows:

S. 1: Initialize the flow solver.

S. 2: Transfer data $(p_{HG}, T_{HG}, \nabla T_{HG})$ provided by the flow solver to the porous medium solver.

S. 3: Converge the porous medium solver.

S. 4: Transfer data $(\vec{v}_{PM}, T_{f,PM})$ from the porous medium solver to the flow solver.

S. 5: Converge the flow solver.

S. 6: Perform grid adaptation in the flow solver.

S. 7: Stop if (19) is fulfilled or return to step 2.

The steps 2 to 5 of this process are illustrated in Fig. 2 together with additional information on the solution procedure in the respective solver.

The system of equations consisting of the compressible Reynolds-averaged Navier-Stokes equations and the Wilcox $k-\omega$ turbulence model is written as $\vec{L}_{HG}(\vec{U}_{HG}) = 0$. Even though we are interested in steady state solutions, we can use the time variable t in the unsteady formulation $\partial \vec{U}_{HG}/\partial t + \vec{L}_{HG}(\vec{U}_{HG}) = 0$ as relaxation parameter in a backward Euler time discretization with the discrete formulation given by

$$(\Delta t)^{-1}\vec{U}_{HG}^{n+1} + \vec{L}_{HG}(\vec{U}_{HG}^{n+1}) = (\Delta t)^{-1}\vec{U}_{HG}^{n}, \quad n = 0, 1, 2, \ldots . \tag{20}$$

The flow solver Quadflow[3] solves the nonlinear system (20) iteratively by using a fully adaptive cell-centered finite volume method on locally refined grids, see Step 5.

The weak formulation for the porous medium system containing the continuity equation, the Darcy-Forchheimer equation and the two heat equations can be written as

$$a^{PM}(\mathbf{U}_{PM}, \mathbf{\Theta}_{PM}) = F(\mathbf{\Theta}_{PM};\, T_{HG}, \nabla T_{HG}), \tag{21}$$

DOI: 10.13009/EUCASS2017-476

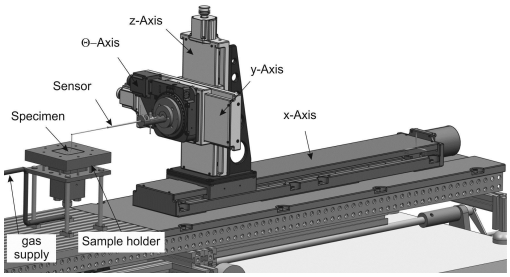

Figure 3: Experimental setup for outflow measurements by Selzer et al.[23]

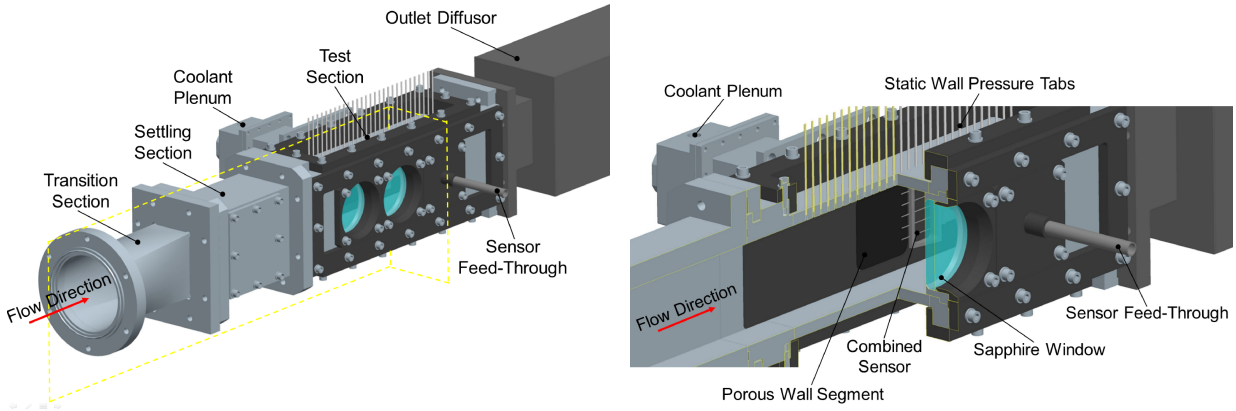

(a) Hot gas channel

(b) Close-up of sample integration

Figure 4: Experimental setup for turbulent hot gas channel flow by Langener et al.[14]

where $a^{PM}(\mathbf{U}_{PM}, \mathbf{\Theta}_{PM})$ is a form that is linear in $\mathbf{\Theta}_{PM}$ and nonlinear in $\mathbf{U}_{PM}$ and $F(\mathbf{\Theta}_{PM};\, T_{HG}, \nabla T_{HG})$ the linear right-hand side functional. The latter incorporates the coupling condition (18) and is therefore dependent on T_{HG} and ∇T_{HG}. By applying operator splitting, the vector $\mathbf{U}_{PM}$ is split into the vectors $\mathbf{U} = (\rho_f, \mathbf{v})$ and $\mathbf{T} = (T_s, T_f)$ such that at first the linear elliptic system

$$a_T(\mathbf{U}^n, \mathbf{T}^{n+1}, \mathbf{\Theta}_{\mathrm{PM}}) = F(\mathbf{\Theta}_{\mathrm{PM}}; T^n_{HG}, \nabla T^n_{HG}) + a_U(\mathbf{U}^n_{\mathrm{PM}}, \mathbf{\Theta}_{\mathrm{PM}}) \tag{22}$$

is solved directly. Subsequently the nonlinear hyperbolic system

$$a_U(\mathbf{U}^{n+1}, \mathbf{T}^n, \mathbf{\Theta}_{\mathrm{PM}}) = F(\mathbf{\Theta}_{\mathrm{PM}}; T^n_{HG}, \nabla T^n_{HG}) + a_T(\mathbf{U}^n_{\mathrm{PM}}, \mathbf{\Theta}_{\mathrm{PM}}) \tag{23}$$

is solved iteratively. For this purpose, a finite element solver has been implemented using the deal.II library.[2] The discretizations and the derivation of the weak formulation for the finite element scheme used in the porous medium solver are discussed in detail in.[6,7,9]

Table 1: Hot gas inflow and cooling conditions.

Mach number	M_∞	0.3
density	ρ_∞	$0.78\,kg/m^3$
temperature	T_∞	$425\,K$
pressure	p_∞	$95\,200\,Pa$
reservoir pressure	p_R	$334\,000\,Pa$
coolant reservoir temp.	T_c	$304.2\,K$
backside temperature	T_b	$321.9\,K$

Table 2: List of porous medium parameters.

throughflow direction		parallel
porosity	φ	0.111
effective heat conduct.	κ_s	$13.5\,W/(mK)$
permeability	K_D	$3.57 \times 10^{-13}\,m^2$
Forchheimer coefficient	K_F	$5.17 \times 10^{-8}\,m$
heat transfer coefficient	h	$10^6\,W/(m^2K)$

4. Numerical Results

In this section, we study the difference between uniformly and non-uniformly simulated cooling gas injection into a subsonic turbulent hot gas channel flow. At first, the experimental setups for the investigation of the turbulent channel

DOI: 10.13009/EUCASS2017-476

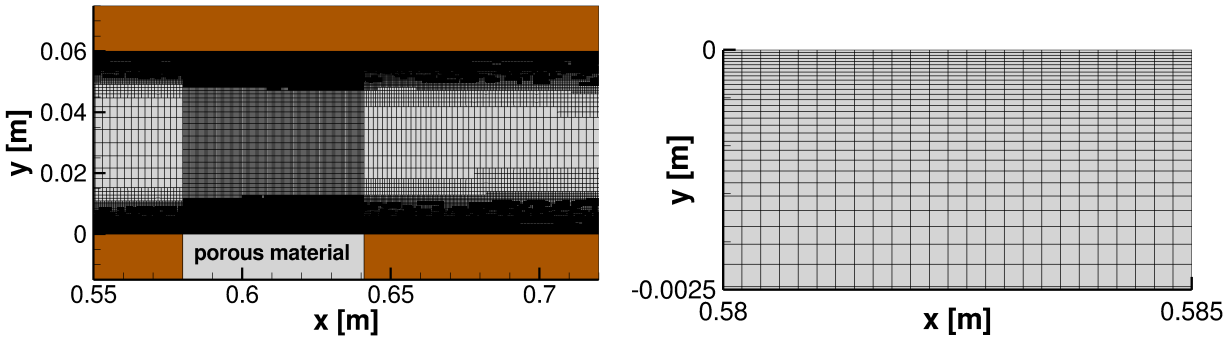

(a) Detail of adaptive grid for hot gas flow.

(b) Detail of grid for porous medium flow.

Figure 5: Details of final grids.

flow and the characteristics of the porous material, respectively, are briefly described in Sect. 4.1, followed by the numerical setup in Sect. 4.2 and the simulation results in Sect. 4.3.

4.1 Experimental Setup

Selzer et al.[23] measured the outflow characteristics of a porous carbon/carbon (C/C) sample with perpendicular outflow orientation, i.e., the fluid in the porous medium has to flow around the carbon fiber bundles. These measurements were carried out with a pitot tube providing local pressure values from which the corresponding velocities could be derived. The pitot sensor was moved in meanders over the sample with a step size of 0.2 *mm*. In total, an area of $10\,mm \times 10\,mm$ was measured. The setup is illustrated in Fig. 3.

For our coupled simulation, we use a setup corresponding to the experiments described .[14,21] Here, a porous C/C sample is mounted into the sidewall of a subsonic wind tunnel. On the backside of the porous material, a coolant reservoir is attached. This experimental setup is shown in Fig. 4. The test section is 1.32 *m* long with the porous material beginning 0.58 *m* downstream of the entrance, the height is 90 *mm* and the width 60 *mm*. The porous wall sample measures $61\,mm \times 61\,mm$ and is 15 *mm* thick. In Dahmen et al.,[7] we compared the results of a single experimental configuration with simulation results. The flow conditions in the hot gas channel and for the cooling gas for this configuration are listed in Tab. 1. Parameters of the porous material are given in Tab. 2. Note that the heat transfer coefficient h can only be estimated and not measured.

4.2 Numerical Setup

Even though the setup and the porous sample of the outflow measurements are different compared with those used for the turbulent hot gas channel experiment, we use the velocity results of the outflow measurements for a coupled simulation with non-uniform injection. The porous samples are not the same, but we can still use the velocity distribution as a typical distribution. The original measurement refers to a 2D interface. Here we take an (arbitrary) line of interface measurement of length 10 *mm* and use it periodically for the simulated porous wall sample of length 61 *mm*. This leads to a total number of 306 velocity values.

First, the non-uniform simulation is carried out up to a steady state regarding the coupled solution. From that simulation, we obtain a resulting average value for the coolant mass flux of $\dot{m}_{c,\mathrm{avg}} = 0.875\,g/s$ leaving the porous medium. This is then used as input value for the uniform simulation by prescribing this value in the coupling condition (17b).

The coarse grid for the flow solver comprises 108 000 grid cells. The grid lines are concentrated towards the walls using a stretching function. The final adaptive grid after 14 coupling iterations and, hence, adaptations consists of about 770 000 grid cells, see Fig. 5(a).

The porous material is discretized by a coarse grid with 306×65 degrees of freedom such that the grid has one grid point per measurement point. The grid lines are concentrated towards the hot gas and towards the reservoir side by applying a stretching technique. The upper left corner of the grid is depicted in Fig. 5(b).

Due to the adaptations of the grid for the hot gas flow, the number of grid points does not agree with the number of measurement points (306) and with the number of porous medium grid points. Hence, the coupling values (13) - (18) are interpolated.

DOI: 10.13009/EUCASS2017-476

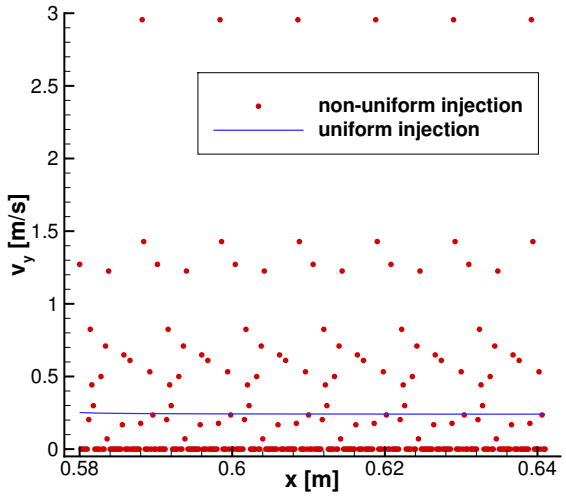

Figure 6: Porous medium flow: normal component of Darcy velocity prescribed by $v_y = v_{y,\text{measured}}(x)$ (non-uniform case) and computed according to (17b) (uniform case) at the interface Γ_{Int}.

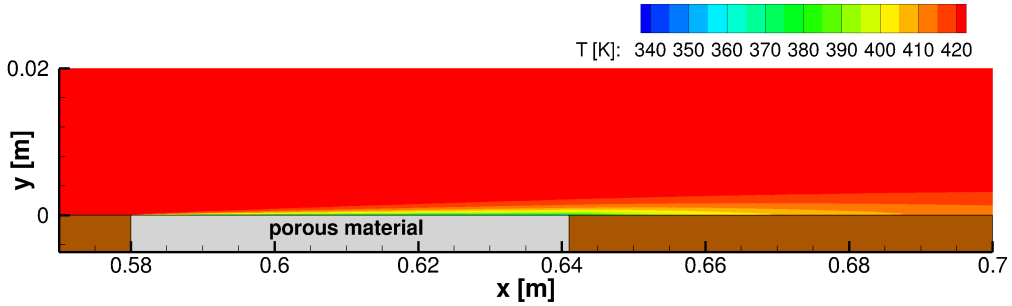

(a) non-uniform injection

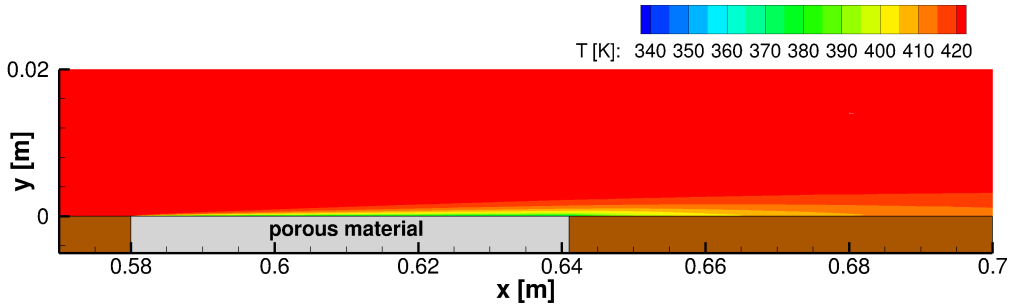

(b) uniform injection

Figure 7: Hot gas flow: temperature.

4.3 Simulation Results

Figure 6 shows the normal component of the porous medium Darcy velocity at the interface to the hot gas flow. In the case of non-uniform injection, the values are directly prescribed as boundary condition, whereas the velocity is computed according to (17b) in the case of uniform injection. Along the porous medium interface, the computed normal velocity values incorporating the constant average mass flux are nearly constant since the density exhibits only small changes due to the small Mach number of 0.3. The deviation between the average values of $0.2399\,m/s$ (non-uniform) and $0.2425\,m/s$ (uniform) is about 1.1 %.

The cooling film in the hot gas flow is depicted in Fig. 7. Its thickness increases over the length of the porous sample. Downstream of the trailing edge, the temperature in the coolant layer increases, mainly due to turbulent mixing. A difference between the non-uniform and the uniform case is hardly visible. In contrast, the close-ups of the cooling film directly downstream of the leading edge of the porous medium in Fig. 8 and further downstream in Fig. 9

DOI: 10.13009/EUCASS2017-476

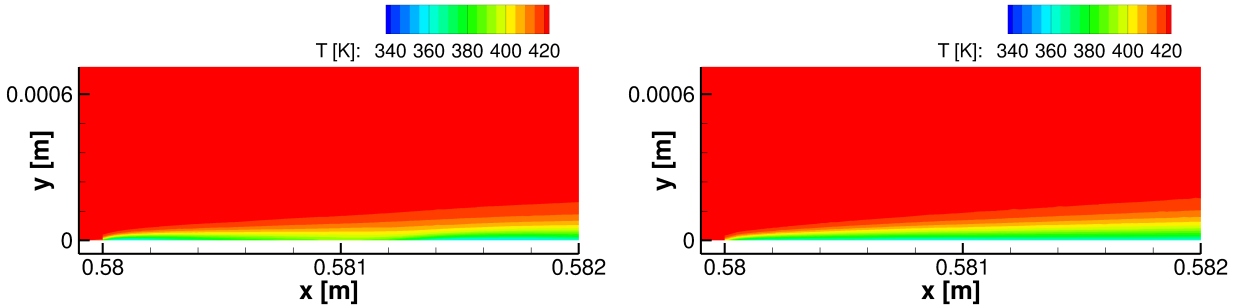

(a) non-uniform injection (b) uniform injection

Figure 8: Hot gas flow: temperature of the developing cooling film directly downstream of the leading edge of the porous medium.

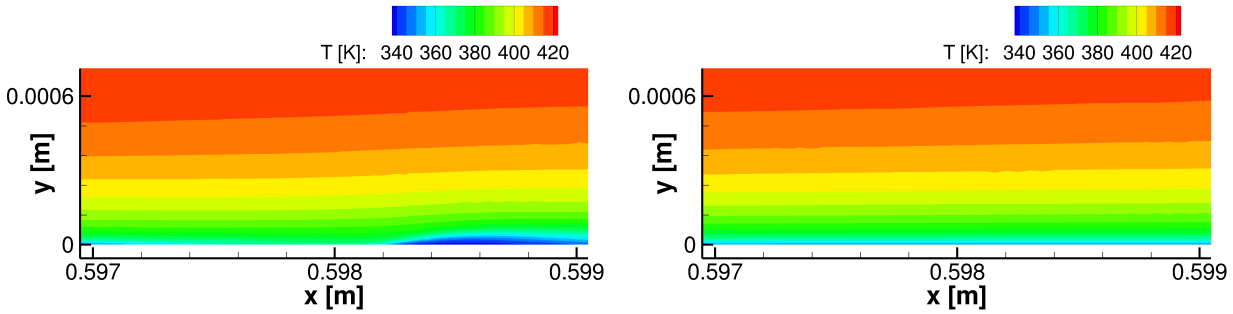

(a) non-uniform injection (b) uniform injection

Figure 9: Hot gas flow: temperature of the cooling film further downstream of the leading edge of the porous medium.

reveal that the cooling film for non-uniform injection develops in a wavelike form and that it has areas of more and of less cooling. The overall effect of the cooling gas injection, however, is very similar as the height of the cooling film indicates and as already seen in Fig. 7.

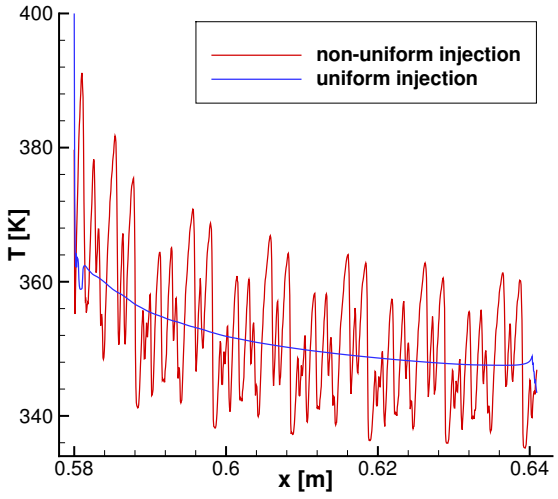

Figure 10: Hot gas flow: temperature at the interface Γ_{Int}.

The same trend can be seen in Fig. 10 for the hot gas temperature along the interface. Single values differ up to 25 K, but the average values are 352.38 K (non-uniform) and 351.35 K (uniform), resulting in a deviation of about 0.3 %.

Other values like the hot gas pressure or the coolant mass flux along the interface confirm the agreement between the average values. The average pressures, see Fig. 11, are 95.643 kPa (non-uniform) and 95.632 kPa (uniform) such

DOI: 10.13009/EUCASS2017-476

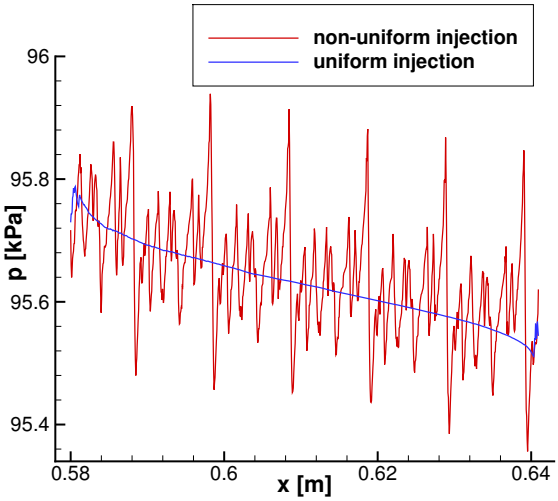

Figure 11: Hot gas flow: pressure at the interface Γ_{Int}.

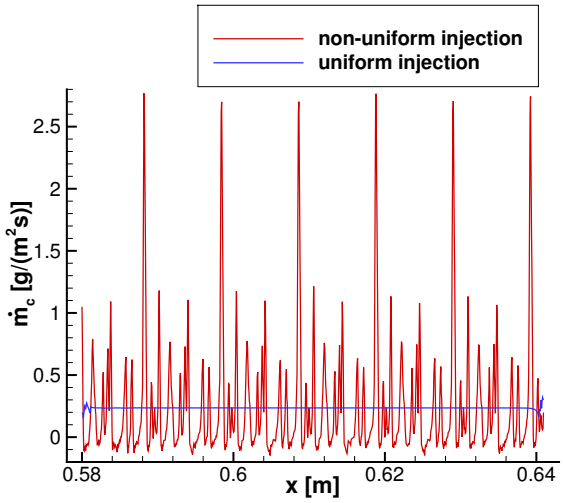

Figure 12: Hot gas flow: coolant mass flux at the interface Γ_{Int}.

that the deviation is approximately 0.01 %. For the coolant mass flux, see Fig. 12, the values are 0.2354 $g/(m^2\,s)$ (non-uniform) and 0.2349 $g/(m^2\,s)$ (uniform) with a resulting deviation of 0.2 %. The mass flux of 0.875 g/s related to the whole porous surface area, prescribed in the uniform case in coupling condition (17b), is well reproduced by the simulation: multiplying the value 0.2349 $g/(m^2\,s)$ with the surface area of 0.061 $m \times 0.061\,m$ leads to $\dot{m}_{c,\text{avg}} = 0.8741\,g/s$, i.e., a deviation of the prescribed value of 1 %.

Figure 13 shows the solid temperature in the porous material. At the interface to the channel, the solid structure and, hence, the coolant is hotter at the leading edge of the porous medium and cooler downstream because of the developing cooling film in the channel. Similarly to the cooling film in the hot gas flow, the temperature distribution shows the expected wavelike behavior. The difference between the two contour plots is shown in Fig. 14, i.e., the absolute value $\left|T_{s,\text{non-uniform}}(x,y) - T_{s,\text{uniform}}(x,y)\right|$ is visualized. One can clearly see the hotter spots at the interface, where no or only a small amount of cooling gas is injected into the hot gas flow in the case of non-uniform injection.

The fluid temperature distribution in the porous medium at the interface is illustrated in Fig. 15. For non-uniform injection, the oscillations are not as large as for the hot gas temperature, cf. Fig. 10. This can also be seen in Fig. 14 in which the maximum difference is about 6 K. The difference between the average value of non-uniform injection and the average value of uniform injection, however, is larger. The values are 340.13 K (non-uniform) and 343.55 K (uniform), leading to a percentaged deviation of 1.01 % which is still small.

DOI: 10.13009/EUCASS2017-476

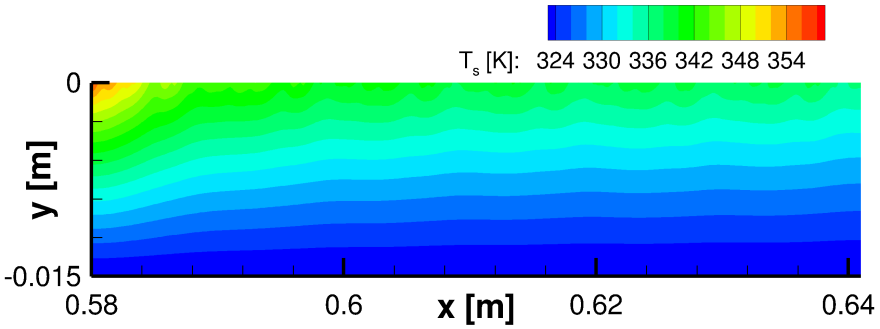

(a) non-uniform injection

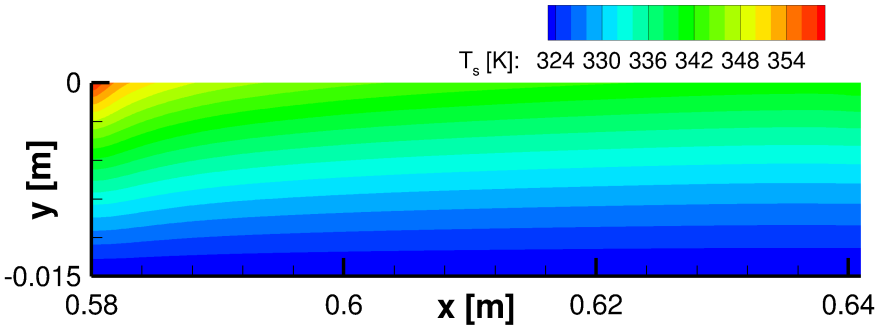

(b) uniform injection

Figure 13: Porous medium flow: solid temperature.

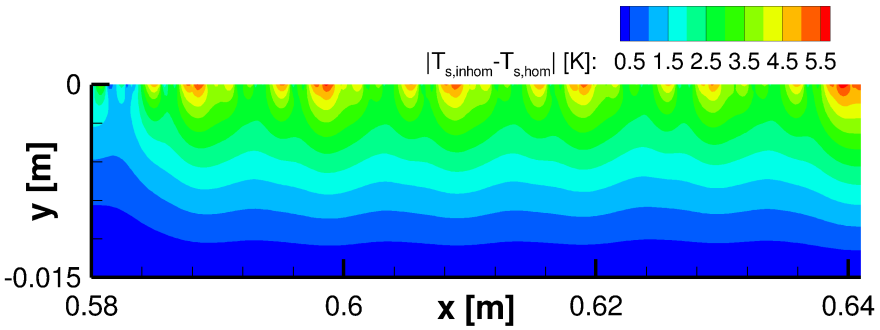

Figure 14: Porous medium flow: absolute difference $\left|T_{s,\text{non-uniform}}(x,y) - T_{s,\text{uniform}}(x,y)\right|$ of the solid temperature.

5. Conclusion and Outlook

In previous work on the numerical simulation of transpiration cooling,[6,7] cooling gas has been injected uniformly by using an averaged coolant mass flux. Due to the porosity of the porous medium the coupling interface is not a smooth surface. As a first step towards accounting for the influence of the surface roughness in our model we here perform computations using a non-uniform mass flux. For this purpose we prescribe outflow velocity data measured along a porous medium in small intervals.

The non-uniform injection appears not to show any significant effect on the cooling film in the hot gas flow, whereas the influence on the temperature of the coolant in the porous medium is much more pronounced. So far, these computations were only performed in 2D. In the future, 3D simulations for non-uniform injection have to be performed. Furthermore, it remains to verify the observations also for realistic conditions in a rocket combustion chamber.

Since direct numerical simulations of the roughness require an extremely high resolution, we want to employ multiscale techniques to model the influence of the roughness on macroscopic quantities without resolving the micro-scale roughness. Currently, we are developing a multiscale concept based on homogenization techniques that is motivated by investigations of Jäger et al.[11] and Achdou et al.[1] for incompressible flows at low Reynolds numbers and, more recently, by Deolmi et al.[8] for compressible laminar flows.

DOI: 10.13009/EUCASS2017-476

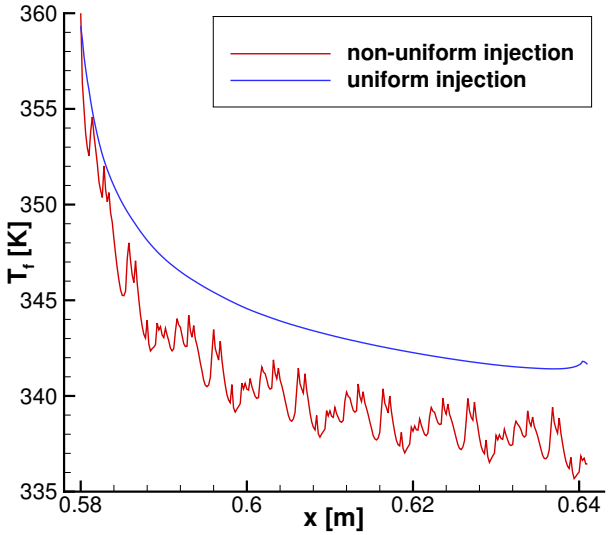

Figure 15: Porous medium flow: fluid temperature at the interface Γ_{Int}.

6. Acknowledgments

Financial support has been provided by the German Research Foundation (Deutsche Forschungsgemeinschaft – DFG) in the framework of the Sonderforschungsbereich Transregio 40.

The authors would like to thank Prof. Dr. J. von Wolfersdorf and S. Schweikert, University of Stuttgart, as well as Dr. H. Hald and M. Selzer, DLR Stuttgart, for fruitful discussions on the modeling of porous medium flow as well as on the coupling problem and for providing us with experimental data.

References

[1] Y. Achdou, O. Pironneau, and F. Valentin. Effective boundary conditions for laminar flows over periodic rough boundaries. *Journal of Computational Physics*, 147:187–218, 1998.

[2] W. Bangerth, R. Hartmann, and G. Kanschat. deal.ii - a general-purpose object-oriented finite element library. *ACM Transactions Mathematical Software*, 33(4):24/1–24/27, 2007.

[3] F. Bramkamp, P. Lamby, and S. Müller. An adaptive multiscale finite volume solver for unsteady and steady state flow computations. *Journal of Computational Physics*, 197(2):460–490, 2004.

[4] W. Dahmen, V. Gerber, T. Gotzen, and S. Müller. Numerical simulation of effusion cooling through porous media. In *5th European Conference for Aeronautics and Space Sciences (EUCASS), Munich*, 2013.

[5] W. Dahmen, V. Gerber, T. Gotzen, S. Müller, M. Rom, and C. Windisch. Numerical simulation of transpiration cooling with a mixture of thermally perfect gases. In *Proceedings of the jointly organized WCCM XI - ECCM V - ECFD VI 2014 Congress, Barcelona*, pages 3012–3023, 2014.

[6] W. Dahmen, T. Gotzen, S. Müller, and M. Rom. Numerical simulation of transpiration cooling through porous material. *International Journal for Numerical Methods in Fluids*, 76(6), 2014.

[7] W. Dahmen, S. Müller, M. Rom, S. Schweikert, M. Selzer, and J. v. Wolfersdorf. Numerical boundary layer investigations of transpiration-cooled turbulent channel flow. *International Journal of Heat and Mass Transfer*, 86, 2015.

[8] G. Deolmi, W. Dahmen, and S. Müller. Effective boundary conditions for compressible flows over rough boundaries. *Mathematical Models and Methods in Applied Sciences*, 25(7):1257–129, 2015.

[9] T. Gotzen. *Numerical Investigation of Film and Transpiration Cooling*. PhD thesis, RWTH Aachen University, 2013.

DOI: 10.13009/EUCASS2017-476

[10] A. Herbertz and M. Selzer. Analysis of coolant mass flow requirements for transpiration cooled ceramic thrust chambers. *Trans. JSASS Aerospace Tech. Japan*, 12(29):31–39, 2014.

[11] W. Jäger and A. Mikelic. On the roughness-induced effective boundary conditions for a viscous flow. *Journal of Differential Equations*, 170:96–122, 2001.

[12] P. Jiang, L. Yu, J. Sun, and Y. Wang. Experimental and numerical investigation of convection heat transfer in transpiration cooling. *Applied Thermal Engineering*, 24:1271–1289, 2004.

[13] T. Langener. *A Contribution to Transpiration Cooling for Aerospace Applications Using CMC Walls*. PhD thesis, Stuttgart University, 2011.

[14] T. Langener, J. v. Wolfersdorf, M. Selzer, and H. Hald. Experimental investigations of transpiration cooling applied to C/C material. *International Journal Thermal Sciences*, 54:70–81, 2012.

[15] J. Linn, M. Keller, and M. J. Kloker. Effects of inclined blowing on effusion cooling in a Mach-2.67 boundary layer. Annual Report SFB TRR40 2010. Munich.

[16] J. Linn and M. J. Kloker. Numerical investigations of film cooling and its influence on the hypersonic boundary-layer flow. In A. Gülhan, editor, *RESPACE - Key Technologies for Reusable Space Systems, NNFM*, volume 98, pages 151–169. Springer, 2008.

[17] J. Linn and M. J. Kloker. Effects of wall-temperature conditions on effusion cooling in a Mach-2.67 boundary layer. *AIAA Journal*, 49(2):299–307, 2011.

[18] Y. Liu, P. Jiang, Y. Xiong, and Y. Wang. Experimental and numerical investigation of transpiration cooling for sintered porous flat plates. *Applied Thermal Engineering*, 50:997–1007, 2013.

[19] Y. Liu, Y. Xiong, P. Jiang, Y. Wang, and J. Sun. Effects of local geometry and boundary condition variations on transpiration cooling. *International Journal of Heat and Mass Transfer*, 62:362–372, 2013.

[20] M. Ortelt, H. Hald, A. Herbertz, and I. Müller. Advanced design concepts for ceramic thrust chamber components of rocket engines. In *5th European Conference for Aeronautics and Space Sciences (EUCASS), Munich*, 2013.

[21] S. Schweikert, J. v. Wolfersdorf, M. Selzer, and H. Hald. Experimental investigation on velocity and temperature distributions of turbulent cross flows over transpiration cooled C/C wall segments. In *5th European Conference for Aeronautics and Space Sciences (EUCASS), Munich*, 2013.

[22] M. Selzer, T. Langener, H. Hald, and J. v. Wolfersdorf. Production and characterization of porous C/C material. Annual Report SFB TRR40 2009. Munich.

[23] M. Selzer, S. Schweikert, H. Hald, and J. v. Wolfersdorf. Throughflow characteristics of C/C. Annual Report SFB TRR40 2014. Munich.

[24] D. C. Wilcox. Turbulence Modeling for CFD. *DCW Industries Inc., 3rd edition*, 2006.